PERFORMANCE LIMITATIONS OF THE LHC CRYOGENICS: 2012 REVIEW AND 2015 OUTLOOK

L. Tavian, CERN, Geneva, Switzerland

Abstract

Dynamic heat loads are deposited in the LHC cryo-assemblies through several processes, in particular by the circulating and colliding proton beams themselves. Measurements of beam-induced heating were performed on the cryogenic system during the 2012 beam operation, mainly on the beam screens and magnet cold masses. Analyses of the measurements have allowed to correlate the beam-induced heating with the beam parameters, to review the heat deposition scaling laws, to extrapolate data for post-LS1 beam operation for different bunch spacing and to identify cooling limitations and consolidations of critical cryo-assemblies, including the continuous cryostats, the stand-alone magnets and the inner triplets.

INTRODUCTION

Scaling laws have been defined to calculate the dynamic heat loads deposited in the LHC machine mainly on the beam screens and on the magnet cold masses. During the 2012 LHC operation, measurements have been performed at reduced beam energy and beam current allowing verifying the scaling laws, identifying possible local or global cooling limitations and recommending related consolidations.

SCALING LAWS OF DYNAMIC HEAT LOADS

Beam-induced heating on the beam screens

The beam-induced heating on the beam screen circuits are coming from:

- synchrotron radiation *Qsr* from the bending magnet,
- resistive dissipation *Qic* of beam image currents induced in the resistive walls and geometrical singularities of the beam channel,
- impingement of photo-electrons *Qec* accelerated by the beam potential ("electron clouds"),

The corresponding scaling laws are given by the following equations:

$$Qsr = Qsr_{nom} \cdot \left(\frac{E}{E_{nom}}\right)^4 \cdot \frac{Nb}{Nb_{nom}} \cdot \frac{nb}{nb_{nom}} \quad (1)$$

$$Qic = Qic_{nom} \cdot \left(\frac{Nb}{Nb_{nom}}\right)^2 \cdot \frac{nb}{nb_{nom}} \cdot \left(\frac{0.60 \cdot E + 2.80}{E_{nom}}\right)^{0.5} \cdot \left(\frac{\sigma}{\sigma_{nom}}\right)^p \quad (2)$$

where:

- Qsr_{nom}= 0.165 W/m per beam,
- Qic_{nom}= 0.180 W/m per beam,
- *E*, the beam energy with E_{nom}= 7 TeV,
- *Nb*, the bunch population with Nb_{nom}= $1.15 \cdot 10^{11}$ protons per bunch,
- *nb*, the number of bunch with nb_{nom}= 2808 bunches per beam,
- σ, the bunch length with σ_{nom}= 1.06 ns,
- *p*, the bunch length dependence factor with *p*= -1.5 in the LHC Design Report (DR)

The third term of the Equation 2 corresponds to the magneto-resistance effect.

Concerning *Qec*, a scaling law is given after efficient beam cleaning and beam scrubbing, which was not the case during the measurement campaign. Consequently, the corresponding scaling law is not used.

The total beam-induced heating *Qdbs* deposited on the beam screens is given by Equation 3:

$$Qdbs = Qsr + Qic + Qec \quad (3)$$

Dynamic heat loads on the cold-masses

The dynamic heat loads on the cold-masses are coming from:

- nuclear inelastic beam-gas scattering *Qbgs* corresponding to a continuous distributed loss of particles from the circulating beam,
- losses of secondary particles *Qsec*, mostly absorbed at 1.9 K in the magnet cold-mass helium bath close to the high-luminosity experimental areas,
- resistive heating *Qrh* occurring in the non-superconducting sections of the magnet excitation circuits, essentially in splices of the superconducting cables.

The corresponding scaling laws are given by the following equations:

$$Qbgs = Qbgs_{nom} \cdot \frac{Nb}{Nb_{nom}} \cdot \frac{nb}{nb_{nom}} \cdot \frac{E}{E_{nom}} \quad (4)$$

$$Qsec = Qsec_{nom} \cdot \frac{E}{E_{nom}} \cdot \frac{L}{L_{nom}} \quad (5)$$

$$Qrh = Qrh_{nom} \cdot \left(\frac{E}{E_{nom}}\right)^2 \quad (6)$$

where:

-
- $Qbgs_{nom}$= 0.024 W/m per beam
- $Qsec_{nom}$= 182 W per high-luminosity half-insertion
- Qrh_{nom}= 0.10 W/m
- *L*, the luminosity with L_{nom}= 10^{34} Hz/cm^2

The total dynamic heat loads *Qdcm* deposited on the cold masses is given by Equation 7:

$$Qdcm = Qbgs + Qsec + Qrh \quad (7)$$

MEASURMENT OF BEAM INDUCED HEATING ON BEAM SCREENS

A measurement method has been implemented in order to assess the heat loads *Qdbs* deposited on the beam-screen circuits. This method is based on enthalpy balance using the outlet control valve characteristics to assess the cooling-loop mass-flow [1].

Bunch length dependence in the arcs

Two specific runs (run3133 and run3345) have been dedicated to study the bunch length dependence on the beam induced heating. During these runs with 50-ns bunch spacing, the photo-electron impingement is negligible. By making the assumption that the synchrotron radiation *Qsr* follows the scaling law given by Equation 1, *Qic* can be deduced from:

$$Qic = Qdbs - Qsr \quad (8)$$

Figures 1 and 2 show for the 2 runs the corresponding *Qic* evolution in the arcs deduced from equation 8 with *Qdbs* measured and *Qsr* calculated by using Equation 1. For the run3345, as the beam energy remains at injection energy (450 GeV), the *Qsr* is definitely negligible (*Qic* = *Qdbs*). On these Figures, the magenta line corresponds to the average measurement of *Qic* in the arc; the green line corresponds to the best fit of the *Qic* using the scaling law (Equation 2) with:

- p = -2 (to be compared with -1.5 in the DR)
- Qic_{nom} = 0.135 W/m per beam (to be compared with the DR value of 0.180 W/m per beam, i.e. 25 % lower than expected).

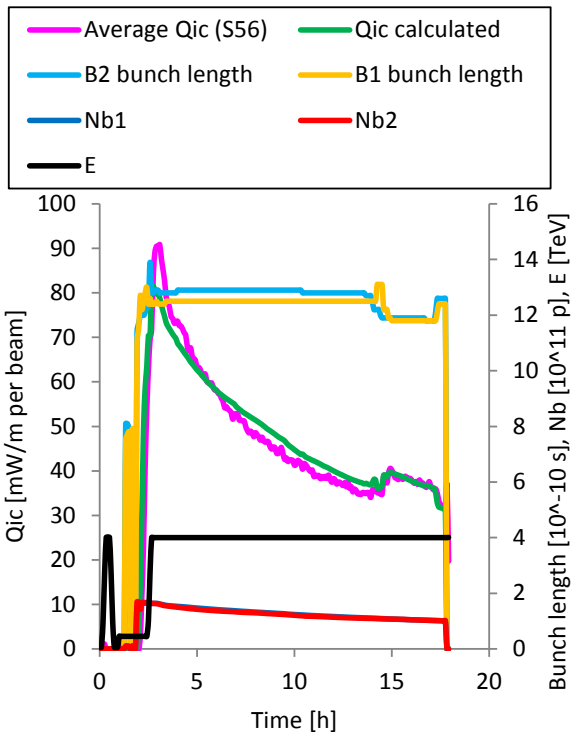

Figure 1: *Qic* evolution in the arcs for run3133

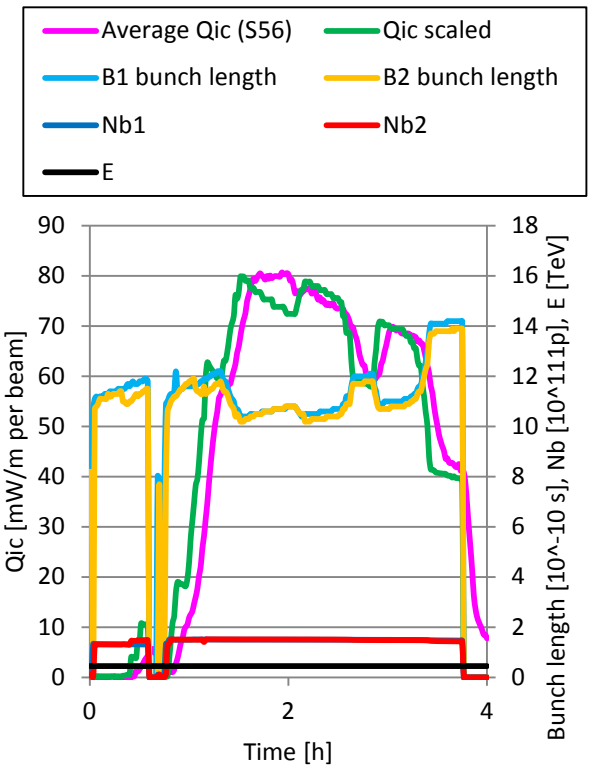

Figure 2: *Qic* evolution in the arcs for run3345

Bunch length dependence in the standalone and semi-standalone magnets

Using the same method, the beam-induced heating on the beam screens of the standalone (SAM) and semi-standalone (Semi-SAM) magnets can be assessed. Figure 3 shows the corresponding Qic evolution for the specific run (run3345).

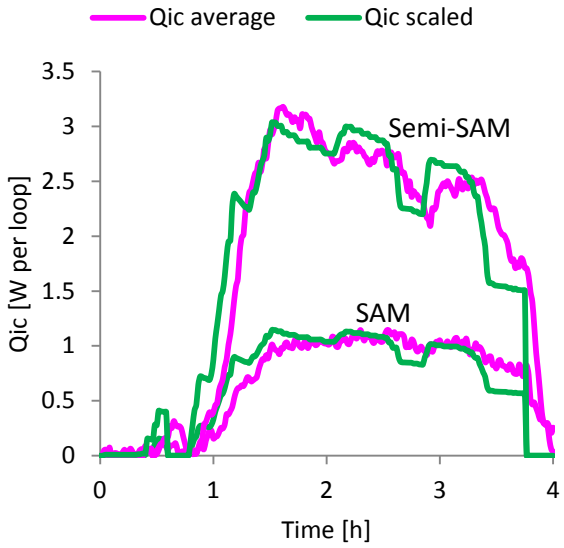

Figure 3: *Qic* evolution in standalone and semi-SAM (run3345)

As for the arc, the best fit corresponds to the scaling law (Equation 2) with:

- p= -2 (to be compared with -1.5 in the DR)
- Qic_{nom}= 0.135 W/m per beam (to be compared with the DR value of 0.180 W/m per beam, i.e. 25 % lower than expected).

Bunch length dependence in the Inner Triplets

Using the same method, the beam-induced heating on the beam screens of the Inner Triplets can be assessed. Figure 4 shows the corresponding Qic evolution for the specific run (run3345).

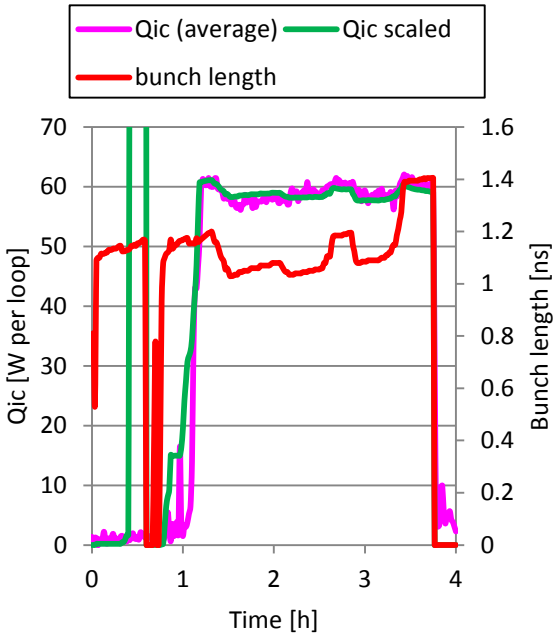

Figure 4: *Qic* evolution in Inner Triplets (run3345)

For Inner Triplets, the best fit corresponds to the scaling law (Equation 2) with:

- p= +0.3 (to be compared with -1.5 in the DR)
- Qic_{nom}= 1.17 W/m per beam (to be compared with the DR value of 0.180 W/m per beam, i.e. a factor 6.5 higher than expected).

Beam-induced heating *Qic* due to image current follows definitely another law in the Inner Triplet than in the rest of the machine. Additional investigation is required to explain this specific behaviour.

Beam-induced heating in the arcs

Beam-induced heating *Qdbs* on the beam screens of the arc half-cells is measured for a typical run (run3134: 4 TeV and 50-ns bunch spacing). Figure 5 shows the evolution of *Qdbs* on a typical sector (S56). The green line corresponds to the scaled evolution with the parameter defined here above (Qic_{nom}= 0.135 W/m per beam and p= -2). As a steady-state cannot be established (beams are continuously loosing protons), an area (see Figure 5) is defined to perform a proofer analysis.

Figure 6 shows the distribution of the Qdbs load on the 8-sector half-cells. The scaled value (green line) is in good agreement with the average value of the distribution.

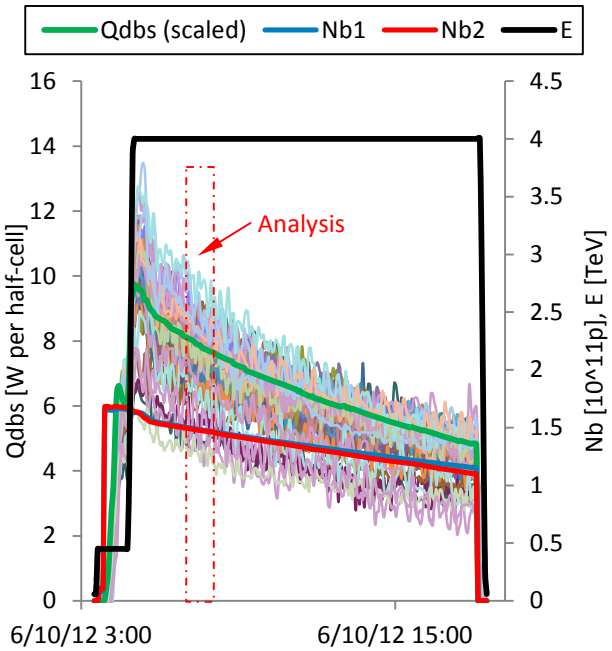

Figure 5: Qdbs evolution in S56 arc half-cells (run3134)

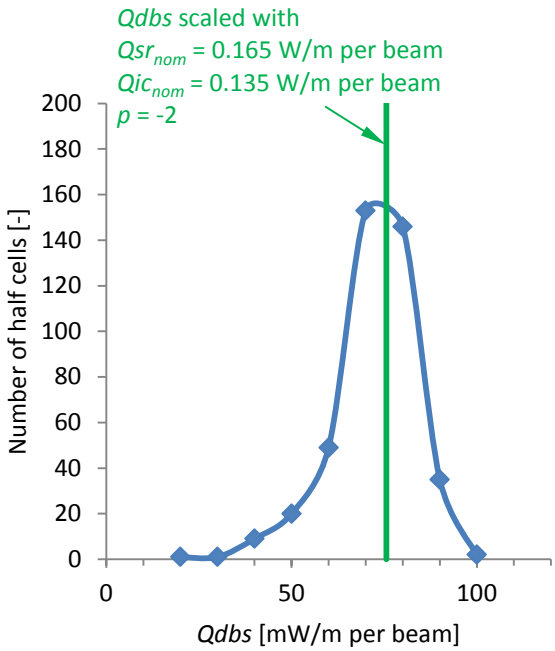

Figure 6: Distribution of Qdbs in the arc half-cells (run3134).

Beam-induced heating in standalone and semi-standalone magnets

Table 1 gives the inventory of standalone (SAM) and semi-standalone (semi-SAM) magnets.

Beam-induced heating *Qdbs* on the beam screens of the SAM and semi-SAM is measured for a typical run

(run3134). Figure 7 shows the distribution of the Qdbs load on the SAM and semi-SAM (data corresponding to the same analysis area than for the arc half-cells). The scaled value (green line) is in good agreement with the average value of the distribution for the semi-SAM. For the SAM the distribution is more erratic and the scaled value slightly over-estimates the average value for SAM. An outlier SAM (Q6R5) has very high beam-induced heating (factor 4.5 higher than the average value). The proximity of the TOTEM detector could be the reason of this overheating (issue under investigation).

Table 1: Inventory of SAM and semi-SAM

Inventory			Length [m]	CV Kvmax [m3/h]
SAM Type 1	Q5R1 Q5R5 Q6L5 Q6L1	Q6R1 Q6R5 Q5L5 Q5L1	8.2	0.02
SAM Type 2	Q6L4 Q4L6 Q5L6	Q6R4 Q4R6 Q5R6	6.9	0.03
	D3L4	D3R4	11.2	
	Q6L2 Q6L7 Q6L3 Q6L8	Q6R2 Q6R7 Q6R3 Q6R8	12.0	
	Q5L2 Q5L8	Q5R2 Q5R8	13.0	
Semi-SAM	Q5D4L4	D4Q5R4	16.7	0.05
	D2Q4R1 D2Q4R5	Q4D2L5 Q4D2L1	19.4	
	Q4D2L2 Q4D2L8	D2Q4R2 Q4D2R8	22.8	

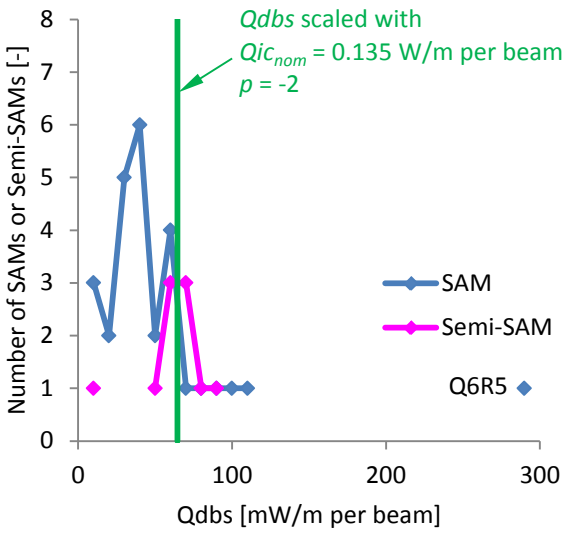

Figure 7: Distribution of Qdbs in SAM and semi-SAM (run3134)

Beam-induced heating in Inner Triplets

Table 2 gives the inventory of Inner Triplets (including the D1 magnets when cold).

Beam-induced heating *Qdbs* on the beam screens of the Inner Triplets is measured for a typical run (run3134). Figure 8 shows the evolution of Qdbs for the Inner Triplets. Figure 9 shows the distribution of the Qdbs load on the Inner Triplets (data corresponding to the analysis area). The scaled value (green line) is in good agreement with the high-luminosity Inner Triplets (IT1 and IT5). Low-luminosity Inner Triplets are significantly lower (up to a factor 1.6 for IT2).

Table 2: Inventory of Inner Triplets

Inventory				Length [m]
ITL1	ITR1	ITL5	ITR5	40
ITL2	ITR2	ITL8	ITR8	50

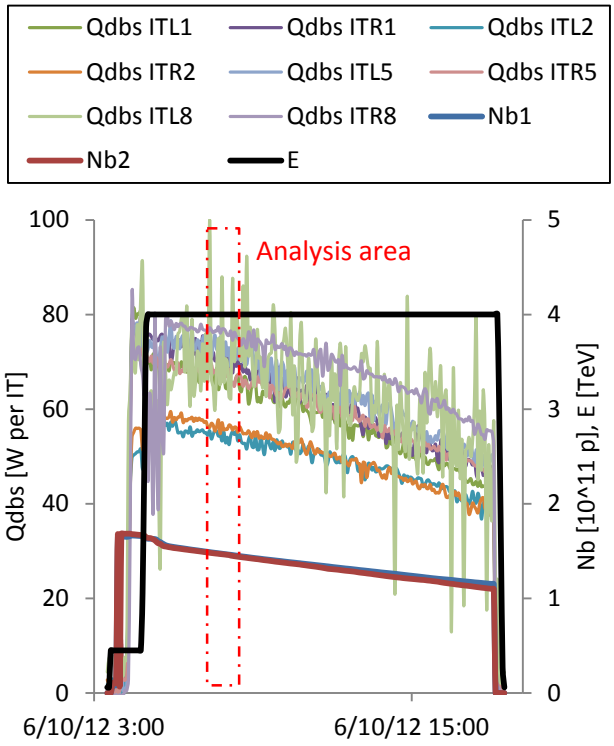

Figure 8: Qdbs evolution in Inner Triplets (run3134)

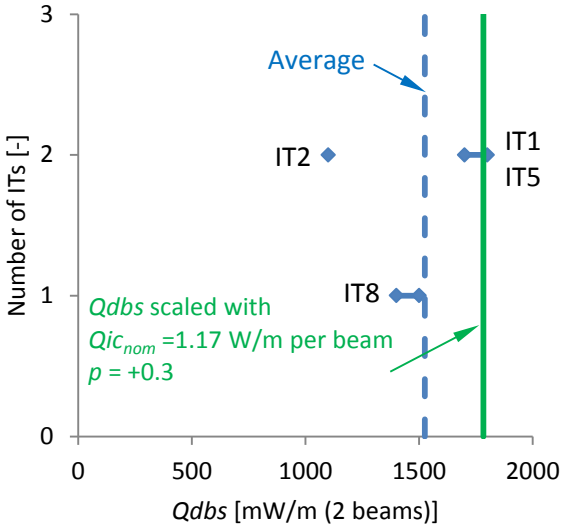

Figure 9: Distribution of Qdbs in Inner Triplets (run3134)

Bunch population dependence

According to the Qic scaling law given by Equation 2, the beam-induced heating due to image current goes with the square of the bunch population *Nb*. Figures 10 and 11 show the measured *Qic* as a function of *Nb* during a typical run for the arc half-cells and for the Inner triplets. The power factor 2 is confirmed for the arc half-cells but is not in accordance with the Inner Triplet for which a power factor of 1.3 is measured.

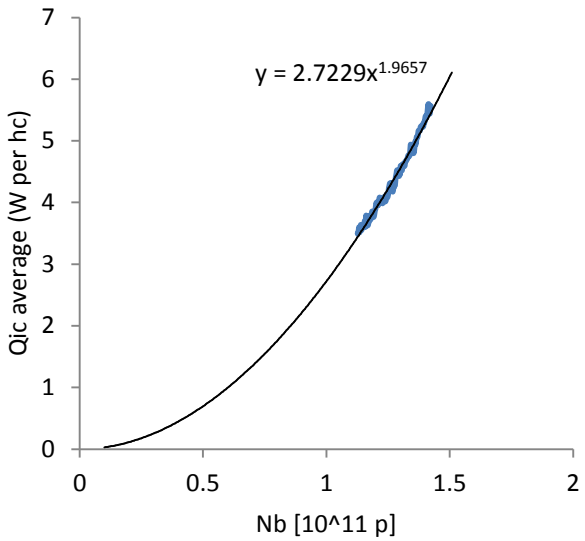

Figure 10: Bunch population dependence of *Qic* for the arc half-cells (run3134)

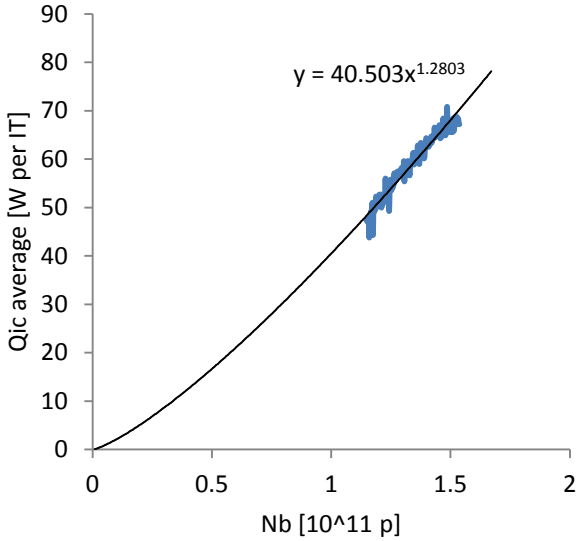

Figure 11: bunch population dependence of *Qic* for the Inner Triplets (run3134)

Scaling for 2015 operation

Two operating scenarios corresponding to bunch spacing of 25 and 50 ns are foreseen during the second physics campaign which will start in 2015. Table 3 gives the corresponding main beam parameters. Beam parameter for the run3134 is also given for comparison.

Table 3: Main beam parameters for 2015

	Run3134	25 ns 2015	50 ns 2015
Nb [p per bunch]	1.49E11	1.15E11	1.6E11
nb [-]	1374	2760	1380
E [TeV]	4	6.5	6.5
σ [ns]	1.29	1.06	1.06
L [Hz/cm^2]	$6.7 \cdot 10^{33}$	10^{34}	10^{34}

Scaling laws with corrected parameter (Qic_{nom} and *p*) can be applied to assess the expected power to be extracted in 2015 for the two 2015 operating scenarios. Table 4 gives the present measured values. Table 5 gives the corresponding total *Qbs* scaled values (including the static heat inleaks *Qsbs*) and the locally installed capacity which is mainly due to the control valve located at the loop outlet. For the arc half-cells of sector S34, the valve poppets were change in 2009 in order to test on a sector the loop controls with a smaller valve, reducing consequently the locally installed capacity in the corresponding arc.

Except for the SAM Q6R5 for which the present capacity is already at the limit, some margins are existing.

Theses margins could be partially or totally used for photo-electron impingement which is present during the beam scrubbing process. Table 6 gives the maximum photo-electron impingement locally acceptable with respect to the present margins.

Table 4: Run3134 measured values [W]

	Qsbs	Qsr	Qic	Total Qbs
Arc half-cell	7.5	1.2	6.9	15.6
SAM type 1	4	0	1.1	5.1
SAM type 2	4	0	1.7	5.7
Semi-SAM	5	0.5	2.9	8.4
SAM Q6R5	10	0	4.8	14.8
IT	5	0.5	71	76

Table 5: *Qbs* scaled values [W]

	25 ns 2015	50 ns 2015	Locally installed
Arc half-cell	34	30	255 (140*)
SAM type 1	6	6	16
SAM type 2	7	7	24
Semi-SAM	16	15	40
SAM Q6R5	20	19	16
IT	114	89	200

*: Data for S34

Table 6: Locally acceptable photo-electron impingement in [W/m per aperture]

	25 ns 2015	50 ns 2015
Arc half-cell	2.1 (1.0*)	2.1 (1.0*)
SAM type 1	0.6	0.6
SAM type 2	0.6	0.6
Semi-SAM	0.6	0.7
SAM Q6R5	N/A	N/A
IT	1.7	2.2

*: Data for S34

25-ns beam scrubbing

A beam scrubbing campaign was scheduled in December 2012 with 25-ns bunch-spacing beams. Figures 12 and 13 show the evolution of the maximum and average photo-electron impingement *Qec* during this campaign.

With respect to the existing margins (given in Table 6 and plotted on the right of the Figures), some limitations are existing for SAM and semi-SAM for which valve poppets and seats have to be changed during the LS1. Concerning the arc of the S34, the maximum values are at the limit and original poppets will be reinstalled in order to recover the same margin present in the other arcs.

The identified limitations seen during this beam-scrubbing campaign are corroborated with the control valve openings which reached 100 % for some of them. Figure 14 shows, as example, the evolution of the Type 1 SAM valve openings.

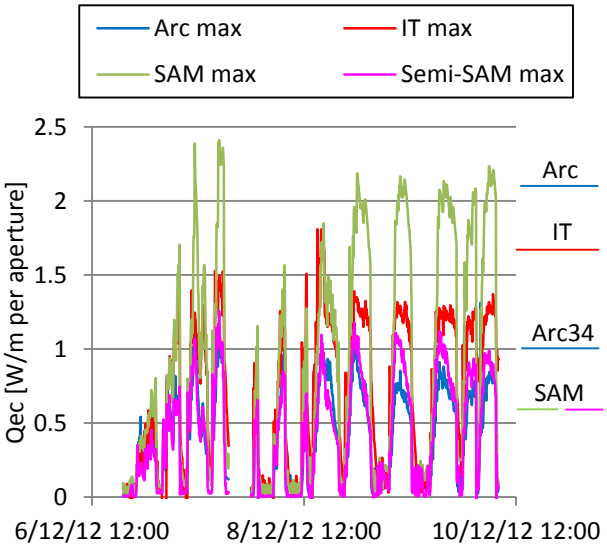

Figure 12: Maximum *Qec* deposition

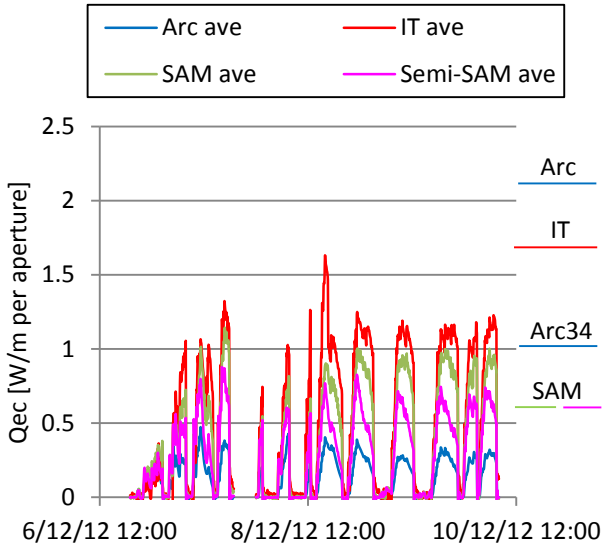

Figure 13: Average *Qec* deposition

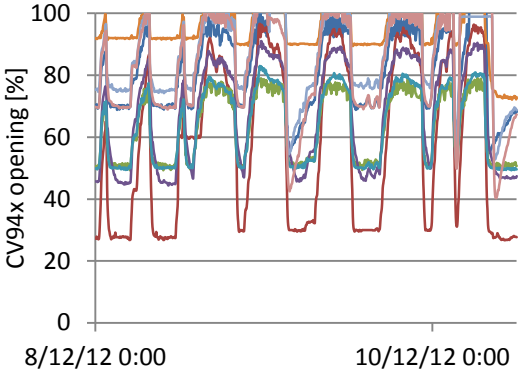

Figure 14: Type 1 SAM valve openings

MEASURMENT OF DYNAMIC HEAT LOAD ON COLD MASSES

Loss of secondary particles in Inner Triplets

The measurement method of the losses of secondary particles in the cold masses of the Inner Triplets is based on the calibration of the extra-opening of the valves controlling the Inner Triplet temperature versus a known electrical heating deposition. Figure 15 shows the calibration of the eight valves. Figure 16 shows the evolution of the losses of secondary particles during the typical run 3134.

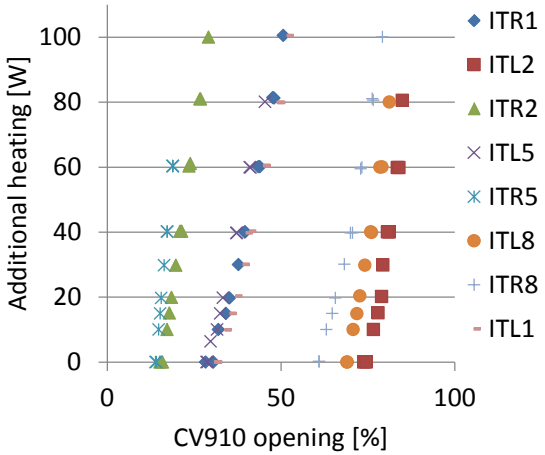

Figure 15: calibration of the IT control valves

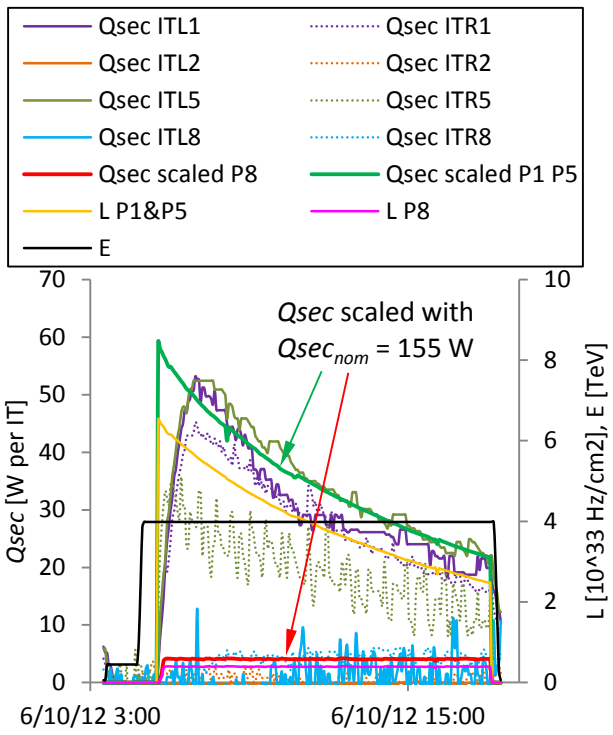

Figure 16: Evolution of secondary particle losses (run3134)

As expected, the losses in the P2 Inner Triplets are negligible (very low luminosity). The secondary particle losses in Inner Triplet at P1 and P5 are significant and show a maximum value around 50 W per IT. In order to scale this evolution according to Equation 5, $Qsec_{nom}$ has to be set at 155 W, i.e. 15 % below the DR value of 180 W. The secondary particle losses at P8 are smaller (~4 W per IT) but are in accordance with the scaled value with a $Qsec_{nom}$ of 155 W.

Dynamic heat load on arc cold masses

The total dynamic heat loads *Qdcm* (loss of secondary particles, beam-gas scattering and resistive heating) can be measured by the variation of the cold compressor pumping flow (S12, S56 & S67) or return module heating (S23). This measurement was only made on the sector equipped with Air Liquide cold compressors given more exploitable data. Figure 17 shows the *Qdcm* evolution for the 4 sectors. At point 6, the same cryoplant is cooling the 2 adjacent sectors (S56 and S67). Consequently, the measured variations correspond to 2-sector heat loads.

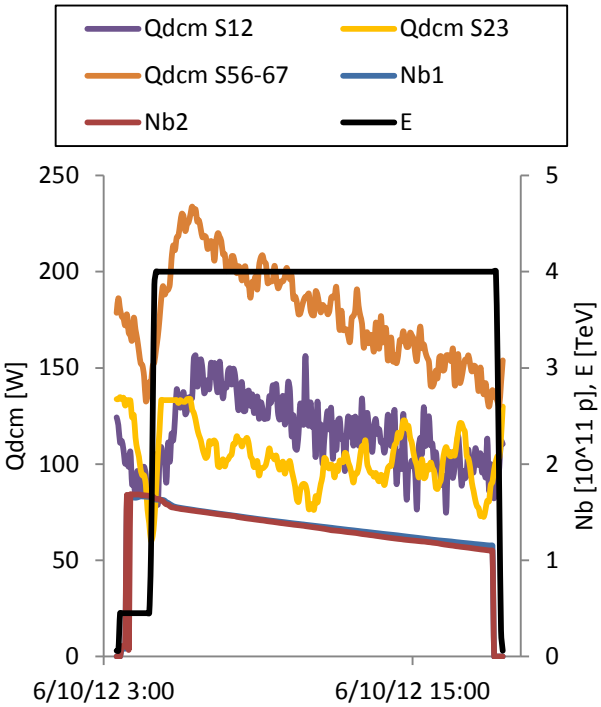

Figure 17: Qdcm evolution for sectors S12, S23, S56 & S67 (run3134)

By subtracting the secondary particle losses measured previously, and by taking into account the length of the concerned cold masses, Figure 18 shows the specific dynamic heat loads in the arc cold masses.

Since the calorimetry [2] performed in 2009 to detect bad splices in the machine, it was shown than the average splice resistance is better than the expected DR data (Qrh_{nom}= 0.10 W/m). The 2009 measured value [3] corresponding to Qrh_{nom}= 0.056 W/m is used in the

scaled evolution (green line in Figure 18) which fits the evolution of the 4 measured sectors.

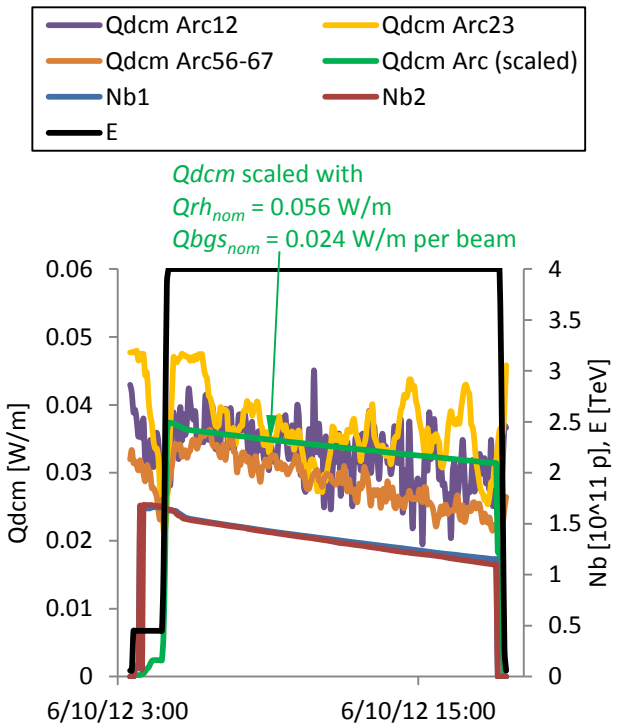

Figure 18: specific *Qdcm* evolution in arc cold masses (run3134)

Scaling for 2015 operation

Scaling laws with corrected parameter ($Qsec_{nom}$ and Qrh_{nom}) can be applied to assess the expected power to be extracted in 2015 for the two 2015 operating scenarios. Table 7 gives the present measured values. Table 8 gives the corresponding total *Qcm* scaled values (including the static heat inleaks *Qscm*) and the locally installed capacity which is mainly due to subcooling heat exchangers capacity or to bayonet heat exchangers (for P1 and P5 Inner Triplets). Table 8 gives also the remaining margins with respect to the local limitations.

Table 7: Run3134 measured values [W]

	Qscm	Qrh	Qbgs	Qsec	Total *Qcm*
Arc cell	18	2.3	2	0.0	22
DS cell	25	1.9	2	0.0	29
ITL1	60	0.5	0.7	60	121
ITR1	52	0.5	0.7	60	113
ITL2	110	0.5	0.9	0.0	111
ITR2	50	0.5	0.9	0.0	51
ITL5	50	0.5	0.7	60	111
ITR5	47	0.5	0.7	60	108
ITL8	80	0.5	0.9	3.6	85
ITR8	46	0.5	0.9	3.6	51

Table 8: *Qcm* Scaled values and remaining margins [W]

	2015 scaled values		Locally installed	2015 remaining margins	
	25 ns	50 ns		25 ns	50 ns
Arc cell	27	26	90(1)	63	64
DS cell	33	32	140(1)	107	108
ITL1	208	208	320(2)	112(3)	112(3)
ITR1	200	200	320(2)	120	120
ITL2	113	112	140(1)	27(3)	28(3)
ITR2	53	52	140(1)	87(3)	88(3)
ITL5	198	198	320(2)	122	122
ITR5	195	195	320(2)	125(3)	125(3)
ITL8	86	86	140(1)	54(3)	54(3)
ITR8	52	52	140(1)	88(3)	88(3)

(1): limited by sub-cooling heat exchanger
(2): limited by bayonet heat exchanger (IT)
(3): could be jeopardized by NC copper braid

Significant margins are existing for arc and DS cells. The identified margins for the Inner Triplet could be jeopardized by non-conformed copper braids on 6 ITs. It is recommended to consolidate these copper braids to fully profit of these extra capacities (Planned for the LS1). Once consolidated, the remaining margins (112 W in ITL1) could be used for higher luminosity production up to $1.75 \cdot 10^{34}$ Hz/cm^2 (scaled from Equation 5).

CRYOPLANT OUTLOOK AND GLOBAL MARGINS

Table 9 recalls the installed refrigeration capacity of the LHC sector cryogenic plants.

Table 9: Installed refrigeration capacity of cryoplants

Temperature level		Installed capacity High-load sectors (S12, S45, S56, S81)	Low-load sectors (S23, S34, S67, S78)
50-75 K	[W]	33000	31000
4.6-20 K (BS)	[W]	7700	7600
4.5 K	[W]	300	150
1.9 K LHe (CM)	[W]	2400	2100
4 K VLP	[W]	430	380
20-280 K	[g/s]	41	27

Figure 19 shows the scaled capacity *Qbs* (25-ns 2015 scenario) required for the beam screen cooling between 4.6 and 20 K. The *Qec* values correspond to the measurements of the December'12 beam scrubbing campaign. The total cooling requirements remain below the installed capacity with margin of about 50 %. A factor 10 is existing between static (only *Qsbs*) and the total cooling requirements. This important factor will certainly create tricky transients both for local and global controls.

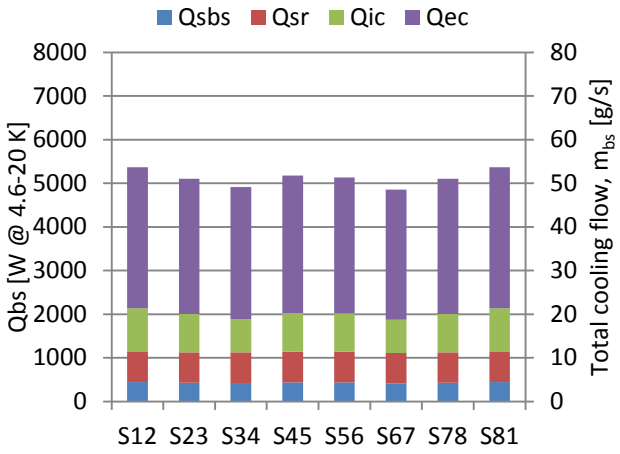

Figure 19: Beam-screen cooling requirement (25-ns 2015 scenario)

Figure 20 shows the scaled capacity *Qcm* (25-ns 2015 scenario) required for the cold-mass cooling at 1.9 K. The total cooling requirements remain below the installed capacity with a large global margin (factor ~2).

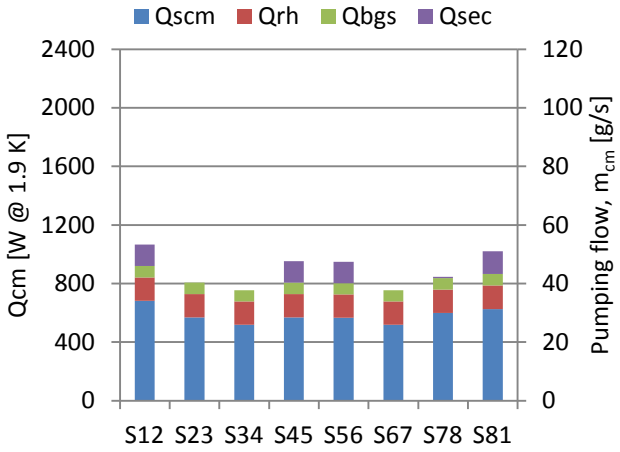

Figure 20: Cold-mass cooling requirement (25-ns 2015 scenario)

Figure 21 shows the arrangement of a cryogenic plant with the two cooling loops for beam screens (BS) and cold masses (CM). These two loop loads are seen by the 4.5-K cryoplant as non-isothermal refrigeration between 4.6 and 20 K. Consequently some capacity sharing is possible. Therefore, the global limitation is when the total flow m_{tot} (= m_{bs} + m_{cm}) reaches the installed flow (197 g/s for high-load sectors and 180 g/s for the low-load sectors). Figure 22 shows the total flow m_{tot} for the different sectors. A cooling margin equivalent to about 90 g/s is existing and corresponds to about 9000 W between 4.6 and 20 K, i.e. about 1.5 W/m per beam for additional dissipation like impingement of photo-electrons, i.e. about 2 W/m per beam available in total for photo-electron impingement (~0.5 W/m per beam already included in the 25-ns 2015 scenario).

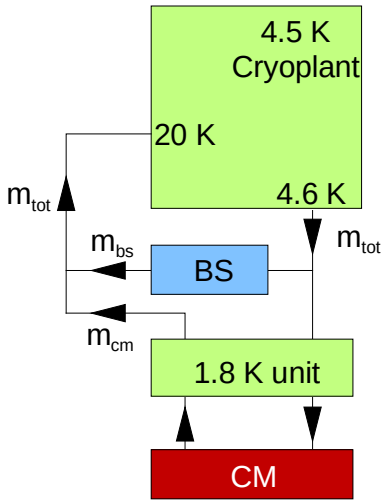

Figure 21: Sector cryoplant arrangement

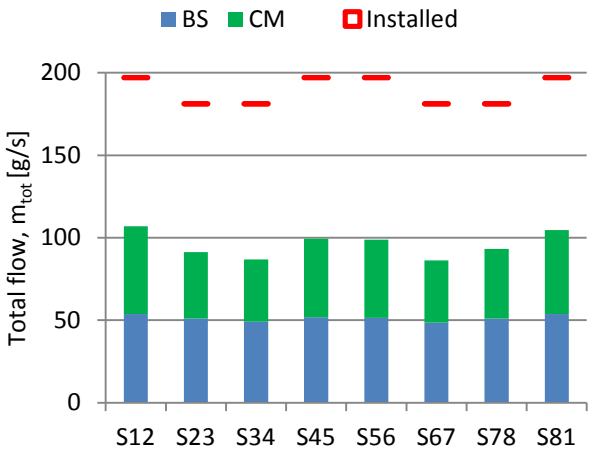

Figure 22: m_{tot} requirement (25-ns 2015 scenario)

CONCLUSION

LHC physics runs have been analysed and dynamic loads have been measured on the beam-screen and 1.9-K cold-mass circuits. Globally dynamic heat loads are below expectation with respect to the Design Report scaling laws except for IT and Q6R5 beam-screen circuits. The scaling laws of dynamic heat loads due to beam-induced heating and splice resistive heating have been refined. Table 10 gives the new working parameters.

A large discrepancy has been identified concerning the resistive dissipation *Qic* of the image current in the Inner Triplets, with:

- a bunch length dependence to the power p= +0.3 (to be compared with p= -2 measured for the rest of the machine and p= -1.5 from the DR).
- a bunch population dependence to the power 1.3 (to be compared with a power factor 2 for the rest of the machine)
- a nominal dissipation of Qic_{nom}= 1.17 W/m per beam (to be compared with 0.135 W/m par beam

measured for the rest of the machine and 0.180 W/m per beam from the DR).

Additional investigation is required to understand this discrepancy. Concerning Q6R5, the proximity of TOTEM roman pots is under investigation.

Table 10: New working data for scaling laws

		DR data	New working data	Delta%
Beam screens	Qsr_{nom} [mW/m per beam]	165	165	0%
	Qic_{nom} (1) [mW/m per beam]	180	135	- 25%
	p (1) [-]	- 1.5	- 2	- 33%
Cold masses	$Qbgs_{nom}$ [mW/m per beam]	24	24	0%
	Qrh_{nom} [mW/m]	100	56	- 44%
	$Qsec_{nom}$ [W per IT]	182	155	- 15%

(1): Not applicable for Inner Triplets

Scaling with 2015 beam parameters shows sufficient margin with respect to local and global cooling limitations by implementing the following consolidations:

- consolidation of the copper braid configuration on 6 over 8 Inner Triplets (planned for LS1). This will allow to efficiently use the 1.9-K cooling margin for luminosity production. However, the maximum luminosity of $1.75 \cdot 10^{34}$ Hz/cm^2 limited today by the consolidated bayonet heat exchanger of the Inner-Triplet cryo-magnets is not in accordance with some simulations showing higher luminosity peak values (up to $2.3 \cdot 10^{34}$ Hz/cm^2).
- increase of the maximum flow coefficient of the beam-screen control valves of the standalone and semi-standalone magnets by exchanging the seat and poppet in order to be compatible with photo-electron impingement of 2 W/m per beam.
- re-installation of the original poppets of the arc34 beam-screen control valves in order to recover the same margin than for the other arcs (to be planned for LS1).

25-ns beam scrubbing run in December 2012 has identified or confirmed:

- a tricky transient to be controlled due to the large dynamic range seen by the 500 local control loops and by the 6 cryoplants. A new control principle is under investigation.
- a discrepancy (about a factor 2) between the cryogenic dynamic heat load measurement (typically 20 kW for the whole machine) and the RF power supply to the beams (typically 40 kW for the two beams). This discrepancy is under investigation by assessing the power dissipated in the warm sections (~3 km) and by assessing the extra capacity supplied by the cryogenic plants during the beam scrubbing run.

ACKNOWLEDGEMENTS

Many thanks to the Cryo-operation team for the tuning of the loops and to Serge Claudet for useful discussions.

REFERENCES

[1] K. Brodzinski and L. Tavian, “First measurements of beam-induced heating on the LHC cryogenic system”, Proc. ICEC24, 2012, pp. 665-668. (CERN-ATS-2013-009)

[2] L. Tavian, “Helium II calorimetry for the detection of abnormal resistive zones in LHC sectors, Proc. PAC’09 Vancouver (2009). (CERN-ATS-2009-006)

[3] G. Ferlin *et al*, “1.9 K heat inleak and resistive heating measurements on LHC cryomagnets” AIP Conf. Proc. 1218 (2010) pp. 1275-1282. (CERN-ATS-2010-016)